

PAPER • OPEN ACCESS

# Validation of TRANSP simulations of the fast deuterium beam distribution in D–<sup>3</sup>He plasmas from (D)–(D<sub>NBI</sub>)–(<sup>3</sup>He) three-ion scheme experiments at JET

To cite this article: Simone Lorenzo Fugazza *et al* 2026 *Plasma Phys. Control. Fusion* **68** 035009

View the [article online](#) for updates and enhancements.

You may also like

- [Collisional–radiative modeling of M1 transition spectra for W<sup>31+</sup>–W<sup>39+</sup> ions within the 500–900 Å range](#)  
Yuting Li, Xiaobin Ding, Ling Zhang *et al.*
- [Physics of the low momentum diffusivity regime in tokamaks and its experimental applicability](#)  
Haomin Sun, Justin Ball, Stephan Brunner *et al.*
- [Nanofoam in action: a versatile tool for laser-plasma interaction experiments](#)  
Alessandro Maffini, Kevin Ambrogioni, David Dellesega *et al.*

# Plasma Physics and Controlled Fusion



## PAPER

### OPEN ACCESS

RECEIVED  
22 October 2025

REVISED  
18 December 2025

ACCEPTED FOR PUBLICATION  
24 February 2026

PUBLISHED  
5 March 2026

Original content from this work may be used under the terms of the [Creative Commons Attribution 4.0 licence](#).

Any further distribution of this work must maintain attribution to the author(s) and the title of the work, journal citation and DOI.



## Validation of TRANSP simulations of the fast deuterium beam distribution in D–<sup>3</sup>He plasmas from (D)–(D<sub>NBI</sub>)–(<sup>3</sup>He) three-ion scheme experiments at JET

Simone Lorenzo Fugazza<sup>1,\*</sup> , Marco Dalla Rosa<sup>1</sup> , Enrico Panontin<sup>2</sup> , Andrea Dal Molin<sup>3</sup> , Jacob Eriksson<sup>4</sup> , Giuseppe Gorini<sup>1,3</sup> , Yevgen Kazakov<sup>5</sup> , Vasily Kiptily<sup>6</sup> , Michal Poradzinski<sup>7</sup> , John Rice<sup>2</sup> , Davide Rigamonti<sup>3</sup> , Mirko Salewski<sup>8</sup> , Žiga Štancar<sup>6</sup> , Marco Tardocchi<sup>3</sup> , Massimo Nocente<sup>1</sup>  and JET Contributors<sup>9</sup> and EUROfusion Tokamak Exploitation Team<sup>10</sup>

<sup>1</sup> University of Milano Bicocca, Department of Physics, Milan, Italy

<sup>2</sup> Massachusetts Institute of Technology, Plasma Science and Fusion Center, Cambridge, MA, United States of America

<sup>3</sup> National Research Council, Institute for Plasma Science and Technology, Milan, Italy

<sup>4</sup> Uppsala University, Department of Physics and Astronomy, Uppsala, Sweden

<sup>5</sup> Laboratory for Plasma Physics—ERM/KMS, Brussels, Belgium

<sup>6</sup> United Kingdom Atomic Energy Authority, Culham Science Centre, Abingdon, United Kingdom

<sup>7</sup> Institute of Plasma Physics and Laser Microfusion, Warsaw, Poland

<sup>8</sup> Technical University of Denmark, Department of Physics, Lyngby, Denmark

<sup>9</sup> See Maggi *et al* 2024 (<https://doi.org/10.1088/1741-4326/ad3e16>) for the JET Contributors.

<sup>10</sup> See Joffrin *et al* 2024 (<https://doi.org/10.1088/1741-4326/ad2be4>) for the EUROfusion Tokamak Exploitation Team.

\* Author to whom any correspondence should be addressed.

E-mail: [s.fugazza2@campus.unimib.it](mailto:s.fugazza2@campus.unimib.it)

**Keywords:** JET Tokamak, gamma-ray, diagnostics, TRANSP simulations, alpha particles, deuterium–Helium-3, three-ion scheme

### Abstract

At JET, Deuterium–Helium-3 (D–<sup>3</sup>He) experiments using ion cyclotron resonance heating (ICRH) with the three-ion scheme were conducted, involving thermal Deuterium (D), thermal Helium-3 (<sup>3</sup>He), and a fast D beam injected via neutral beam injection (NBI) and further heated using ICRH. In these plasmas, intense neutron emission at the level of  $\approx 10^{16}$  n s<sup>-1</sup> was observed, and a non-thermal neutron spectrum was measured with the JET time of flight neutron spectrometer. Furthermore, the spatial profile of  $\approx 16.4$  MeV gamma rays originating from the <sup>3</sup>He(D,  $\gamma$ )<sup>5</sup>Li reaction was observed. This is a weak branch ( $\approx 10^{-5}$  relative probability) of the more common <sup>3</sup>He(D, p) $\alpha$  reaction and it can be used to assess the production of alpha particles in these experiments. In this work we analyse a set of data from nuclear diagnostics in D–D<sub>NBI</sub>–<sup>3</sup>He experiments at JET and compare them with synthetic diagnostics based on TRANSP simulations of the fast deuterium distribution function, using the so-called ‘kick operator’ to model power transfer from the wave to the beam fast deuterons. The neutron rate predicted by the TRANSP simulations broadly agrees with data measured with fission chambers. The shape of the neutron emission spectrum is also well understood, once finite Larmor radius effects are introduced into calculations. Data from the gamma ray camera are used to infer the alpha birth profile through tomographic reconstructions based on the TREVISIO code. These were compared with corresponding calculations starting from TRANSP results and showing an overall good agreement with the experimental tomographies. The validated TRANSP results are finally used to discuss the modifications of the fast deuterium distribution function and of the alpha birth profile in a set of discharges.

## 1. Introduction

The investigation of alpha particles represents one of the most challenging aspects of diagnostics in tokamaks [1]. For energy production, the most promising fusion reaction is the Deuterium–Tritium (DT) reaction, where an alpha particle (in addition to a neutron) is produced, which is anticipated to be the dominant source of heating in burning plasma [2, 3]. Due to their positive charge, alpha particles

are confined by strong magnetic fields and cannot escape the plasma. The detection of confined alpha particles is particularly difficult, as opposed to the lost alpha particles, which can be detected outside the plasma. In addition, alpha measurements in DT plasmas are particularly challenging due to the intense neutron background [4]. This fact suggests the need to look for another method to study alphas.

An important source of alpha particles has been achieved at JET through Deuterium–Helium-3 (D– $^3\text{He}$ ) plasmas, during dedicated experiments known as the ‘Three-Ion Scheme’ [5–8]. In the scheme analysed in the present manuscript, the plasma is made of deuterium and  $^3\text{He}$ , at relative concentrations of 50% and 25%, respectively. The fast ion source comes from neutral beam injection (NBI) of deuterium that absorbs most of the power injected by ion cyclotron resonance heating (ICRH) when the wave frequency is set to match the Doppler shifted ion cyclotron frequency of the deuterium beam in the plasma core [9]. These conditions result in a strong alpha and neutron emission produced by  $^3\text{He}(\text{D},\text{p})\alpha$  and  $\text{D}(\text{D},\text{n})^3\text{He}$  reactions, respectively, with total neutron rates in the range of  $\sim 1 \cdot 10^{16} \text{ n s}^{-1}$ . This emission is expected to be localised in the plasma core and to be significantly lower in the outer regions [10]. This localised and intense alpha source provides a unique opportunity to test alpha diagnostics.

Experimental evidence of the interaction among the three ion species (thermal Deuterium, thermal Helium-3 and the fast Deuterium population) has been obtained at JET. The gamma camera Upgrade [11, 12], equipped with  $\text{LaBr}_3:\text{Ce}$  scintillators [13–15], detects the 16.4 MeV gamma emission from the  $^3\text{He}(\text{D},\gamma)^5\text{Li}$  reaction [16–18]. Information about alpha particles born from  $^3\text{He}(\text{D},\text{p})\alpha$  reactions can be inferred from the 16.4 MeV gamma-ray measurements, as previously performed in [10]. Simultaneously, the TOFOR neutron spectrometer measures neutrons from the  $\text{D}(\text{D},\text{n})^3\text{He}$  reaction [19, 20]. In both diagnostics, the fast deuterium plays a key role in determining the shape and features of gamma and neutron spectra.

These diagnostics provide experimental data from which information on the spatial and energy distribution of alpha particles can be extracted. In parallel, simulations with the TRANSP code [21–23] can be used to predict emission spectra in three-ion scheme scenarios, thereby enhancing our understanding of the underlying physics processes and thus of the alpha emissivity.

The aim of this work was to validate the TRANSP simulations against experimental TOFOR neutron spectra and gamma camera data, from a set of discharges during three-ion scheme experiments. First, we compared the time evolution of the total neutron rate predicted by TRANSP with experimental measurements. Second, we compared neutron time-of-flight (TOF) spectra measured using TOFOR with synthetic spectra computed from the fast deuterium distribution retrieved by TRANSP. Third, we analysed the spatial poloidal profiles of alpha emissivity, both experimental (reconstructed from gamma camera data) and synthetic (calculated from TRANSP outputs). A tomographic reconstruction was then performed using the TREVISO code [24], which implements an iterative inversion algorithm based on the Maximum Likelihood–Expectation Maximization method.

The paper is organized as follows. Section 2 describes the JET instruments (TOFOR and gamma camera) used to collect the experimental data. Section 3 presents the three-ion scheme discharges. The analysis method is outlined in section 4, including the TRANSP simulations under investigation, the procedure to generate synthetic TOFOR neutron spectra, the approach used to derive gamma camera profiles from both experimental and simulated data, and the tomographic method for reconstructing the alpha birth profile. The results are presented in section 5, while their discussion is provided in section 6.

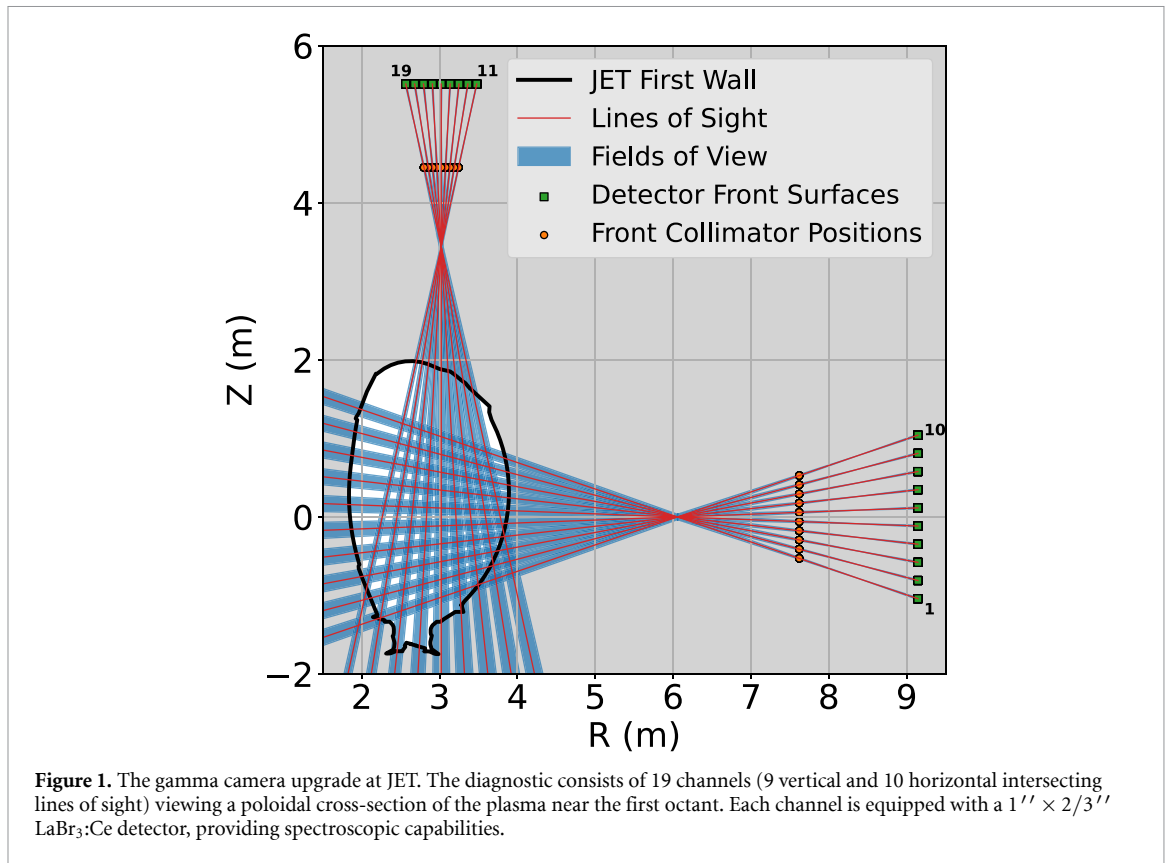
## 2. Instrumentation

### 2.1. The TOF neutron spectrometer at JET

In three-ions scheme experiments, a significant amount of deuterium is present in the plasma, enabling  $\text{D}(\text{D},\text{n})^3\text{He}$  fusion reactions. These produce neutrons with a characteristic energy of approximately 2.5 MeV. In the idealized case of cold deuterium (i.e. negligible kinetic energy), the neutron emission spectrum would be monoenergetic. However, heating mechanisms such as Thermal, NBI, and ICRH introduce distinctive features in the neutron spectrum, which can be detected by dedicated diagnostics [25–27].

TOFOR is a neutron TOF spectrometer at JET, optimized for the detection of DD neutrons with energies around 2.5 MeV [19, 20]. It measures the neutron TOF across a known distance, which is related to the neutron energy via the instrumental response function [28]. For TOFOR, the most likely response is described by:

$$E_n = \frac{2m_n R^2}{\text{TOF}^2} \quad (1)$$



where  $E_n$  is the neutron energy,  $m_n$  is the neutron mass, and  $R = 705$  mm is the radius of the constant-TOF sphere (a fixed geometric parameter of TOFOR). Longer TOF values correspond to lower neutron energies, and vice versa.

TOFOR was designed to achieve an optimal compromise among performance parameters for DD neutron measurements: an energy resolution of  $\Delta E_n/E_n = 5.8\%$ , a geometrical efficiency  $\epsilon = 0.12$  cm<sup>2</sup>, and a count rate  $C_n = 300$  kHz, corresponding to a maximum neutron flux of  $3 \times 10^6$  ns<sup>-1</sup> cm<sup>-2</sup> incident on the entrance detector.

In TOF space, the DD neutron peak (2.5 MeV) typically appears around 65 ns. A narrow peak indicates monoenergetic or thermal emission, while broader spectra are observed when  $\sim 100$  keV NBI ions dominate. In three-ion scheme experiments, spectra are significantly broader and have a non-trivial shape, suggesting a strong contribution to the neutron emission from the fast deuterium population, which dominates both the spectral structure and intensity.

## 2.2. The gamma camera upgrade at JET

Figure 1 shows a schematic of the gamma camera upgrade at JET [11, 12]. The system comprises 19 channels, 10 horizontal and 9 vertical lines of sight, intersecting in a poloidal plane near the first octant of the JET vessel. Each line of sight is equipped with a  $1'' \times 2/3''$  LaBr<sub>3</sub>:Ce scintillator [29], enabling gamma-ray spectroscopy.

The gamma camera diagnostic system can be used to detect gamma-ray emission from the  ${}^3\text{He}(\text{D},\gamma){}^5\text{Li}$  reaction [10, 17]. This is a rare branch of the  $\text{D}-{}^3\text{He}$  fusion reaction that emits a 16.4 MeV photon instead of an alpha particle, with a branching ratio  $\text{BR} \sim 10^{-5} \gamma/\alpha$ . [30]

Observing the spatial distribution of this emission allows us to infer the birth profile of fusion-born alpha particles, and a substantial contribution from fast deuterium is expected in determining this profile. As already stated, the 16.4 MeV gamma-ray emission originates from the  $\text{D}-{}^3\text{He}$  reaction, which also produces alpha particles. If the gamma-per-alpha branching ratio of the  $\text{D}-{}^3\text{He}$  reaction is assumed to remain approximately constant, then the gamma-ray spatial profile directly reflects the alpha-particle birth profile. A similar approach was previously adopted in [10]. [17] indeed reports that the gamma-per-alpha branching ratio remains nearly constant at  $\sim 2.5 \cdot 10^{-5}$  for deuteron energies between 300 and 600 keV, and there is then an almost linear increase up to  $\sim 4.5 \cdot 10^{-5}$  at 900 keV. For the discharges analysed in this paper, we have evaluated that the mean energy of the deuterons that contribute to alpha particle production, weighted by the fusion reactivity, is below 600 keV in most cases and up to 650 keV

**Table 1.** Discharges and associated TRANSP simulations, together with the selected timestamps for fast deuterium distribution analysis.

Shot #	95 671	95 672	95 673	95 679	95 680	95 683	95 684
Simulation ID	A25	A25	A26	V36	V07	V07	A24
Time (s)	10.0	12.0	11.0	9.95	9.95	9.20	9.00

in all cases. Hence, it is expected that the increase of the branching ratio reported in [17] will have little impact on the reconstruction of the alpha particle profile from gamma-ray measurements, which is the focus of this paper. There may be some impact on the determination of the overall absolute alpha particle production rate from measurements, which is however out of the scope of this paper and will be addressed in a separate study.

### 3. Description of discharges

This study analyses seven JET discharges (95 671, 95 672, 95 673, 95 679, 95 680, 95 683, 95 684) performed under similar experimental conditions. These shots are part of the three-ion scheme experiments, characterised by the presence of three ion species in the plasma: thermal deuterium, thermal helium-3, and a fast deuterium population [5, 6]. The fast deuterium is initially injected via NBI at approximately 100 keV and subsequently accelerated through ICRH, reaching energies up to 1–2 MeV. A schematic overview of the heating scheme is shown in figure 2.

All discharges were operated with a plasma current of 2.5 MA and a toroidal magnetic field of -3.7 T. The electron density at the plasma core is around  $1.0 \times 10^{20} \text{ m}^{-3}$ , and the  $^3\text{He}$  concentration varies between 18% and 28%, according to data from the real-time experiment central control (RTCC) system [31]. The electron temperature typically ranges from 1 to 10 keV. The discharge is initially heated by NBI and there is a phase of a few seconds where ICRH is also applied. This is when the three-ion scheme is established and most of neutron and gamma-ray emission is observed. In most cases, the NBI power exceeds the ICRH power by a factor of 2–3, except for discharges 95 673 and 95 684. NBI power ranges from 3.1 to 18.6 MW, while ICRH power varies from 2.1 to 6.1 MW. Across all discharges, the neutron rate reaches values of the order of some  $10^{15} \text{ n s}^{-1}$ , up to about  $10^{16} \text{ n s}^{-1}$ .

An example of the actual waveforms for discharge #95671 is shown in figure 3.

## 4. Analysis method

### 4.1. TRANSP simulations

The TRANSP code [21–23] has been developed to simulate particle and energy transport in tokamak plasmas. In this study, it is used to model the time evolution of the total neutron rate and the fast deuterium distribution during each discharge.

For each pulse, a TRANSP simulation was performed in an iterative manner. Measured plasma parameters, such as the magnetic equilibrium, the profiles of density, temperature, effective ion charge and bolometry, were used as input. The simulations further used the actual heating profile of NBI and ICRH. As in other analyses of radio-frequency heating scenario, the TORIC code was used within TRANSP to simulate wave absorption. A ‘kick operator’ [32] was active to calculate the power transfer from the wave to the beam ions and their acceleration to higher energies. The exact impurity content at JET, mainly Beryllium and Nickel, is uncertain, as is the value of  $^3\text{He}$  concentration, which is estimated at about 20% of the ion density in these discharges. For this reason, these parameters were varied in a number of iterations (namely, TRANSP runs) until a reasonable agreement between the measured and simulated neutron rate and plasma stored energy was achieved. In the discharges analysed here, neutron emission is due to reaction among thermal ions (thermal component), fast ions and thermal ions (beam-target component) and fast ions among themselves (beam-beam component).

For each discharge, the timestamp at which the simulated neutron rate best matches the experimental measurement is identified. The corresponding fast deuterium distribution is then extracted at the selected time (see timestamps in table 1).

TRANSP computes the fast distribution over the full phase space, resolving it in space, time, energy, and pitch. An example for discharge #95671 is shown in figure 4. Panel 4(a) presents the spatial density of fast deuterium (integrated over energy and pitch), while panel 4(b) shows the energy-pitch distribution (integrated over space). A high-energy tail is visible in the positive pitch area, extending from 100 keV to 1–2 MeV.

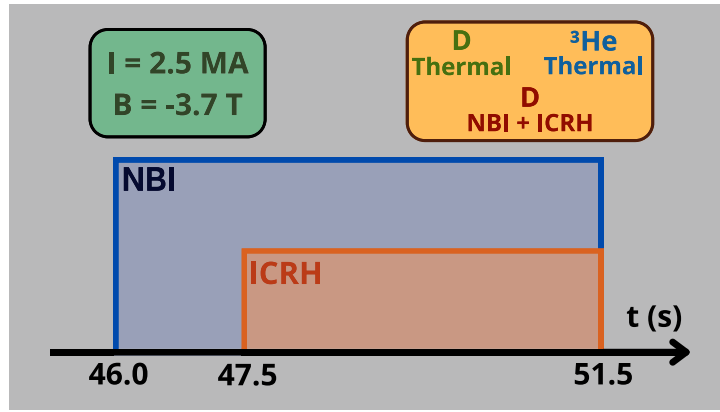


Figure 2. Schematic of the auxiliary heating waveforms in a typical three-ions scheme discharge.

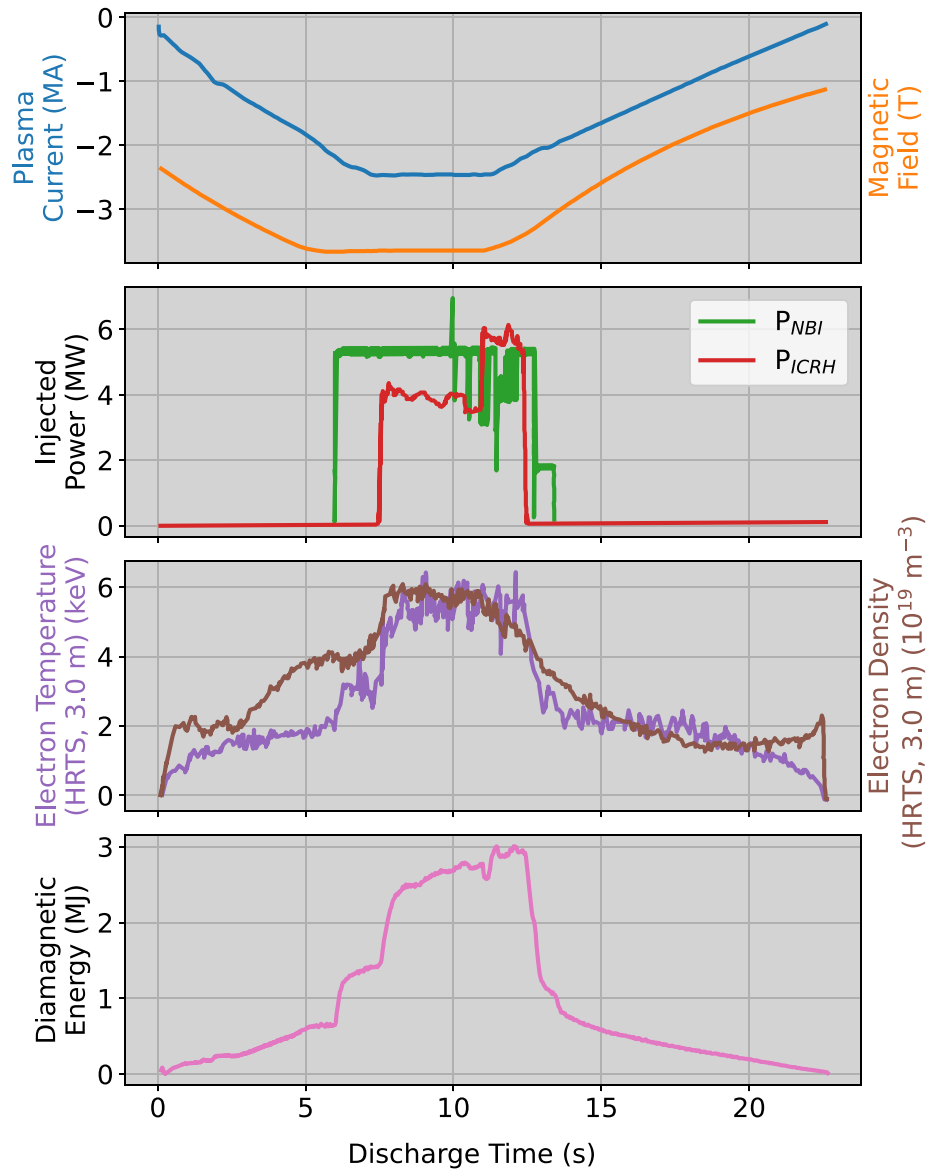
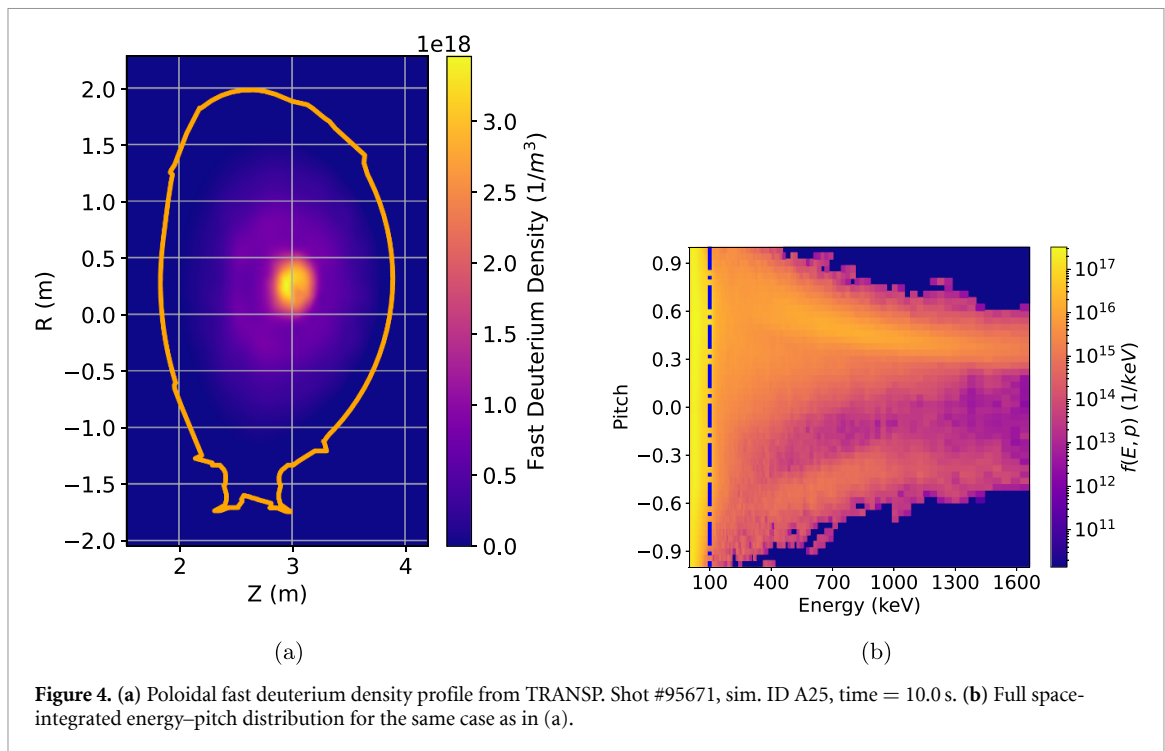


Figure 3. Time traces measured at the plasma core for Discharge #95671, showing: plasma current and magnetic field; NBI and ICRH power; electron temperature (HRTS, 3.0 m) and density (HRTS, 3.0 m); diamagnetic energy. Time offset of 40 s.



The errors of the TRANSP outputs are likely underestimated as they originate in part from the interpolation of data affected by significant experimental uncertainties. However, for the purposes of this work, we deemed it appropriate to regard them as not reliably assessable using only the estimation method previously described and, instead, focused on building a functional framework. One of the next planned upgrades will be to evaluate the impact of these errors on the performed simulations.

#### 4.1.1. Synthetic neutron spectra

The fast deuterium distribution (see figure 4) is extracted at the selected timestamp (see table 1) for each simulation and it is used to calculate the expected time of flight spectrum along the line of sight of the TOFOR neutron spectrometer and for comparison with data obtained with this instrument.

The validation process begins by extracting TOFOR neutron energy spectra at each timestamp, using a time window of 0.8 s centred around the selected time point. Synthetic spectra are then generated using the GENESIS Monte Carlo code [33] and convolved with the TOFOR response function for comparison with experiment. Thermal deuterium profiles (density and temperature), magnetic equilibria and the fast deuterium distribution are taken from TRANSP outputs, while the TOFOR line of sight file was calculated using the LINE2.1 code [34].

To accurately model the TOFOR spectrum, all relevant neutron-producing interactions must be included. Reactions involving fast deuterons dominate due to their higher energies and larger cross sections compared to thermal reactions. The fast deuteron population is artificially divided into two components: a low-energy (Lfast) and a high-energy (Hfast) group, identified based on whether their energies are higher or lower than a 100 keV threshold (see the dashed blue line in figure 4(b)). The Lfast population is attributed mainly to NBI, while Hfast originates from ICRH heating and reaches energies up to 1–2 MeV.

Six interaction channels contribute to the total spectrum:

- Thermal–Thermal (ThTh)
- Thermal–Lfast (ThLf)
- Thermal–Hfast (ThHf)
- Lfast–Lfast (LfLf)
- Hfast–Lfast (HfLf)
- Hfast–Hfast (HfHf)

Among these, Hfast-related channels are expected to dominate both the spectral shape and neutron yield.

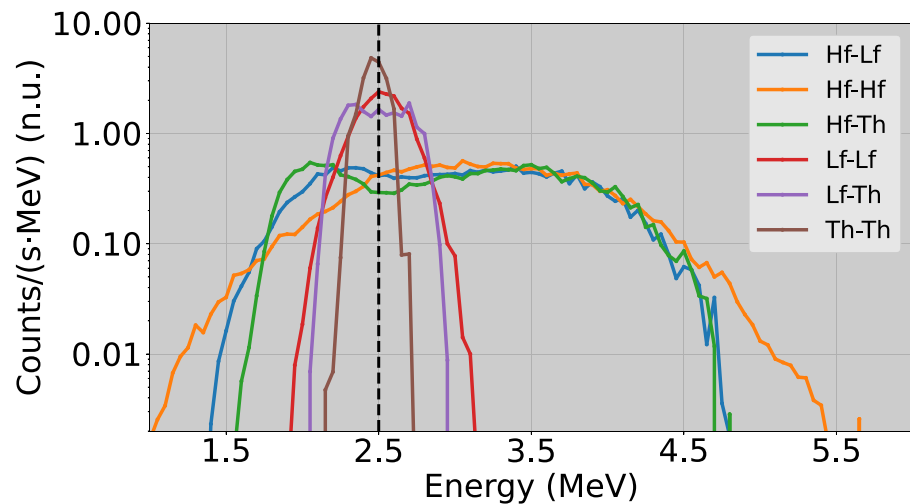


**Figure 5.** Normalised neutron spectral components from orbit-corrected simulations (TOFOR diagnostic, energy-resolved). Shot #95671, simulation ID A25, discharge time = 10 s.

TRANSP fast distribution simulations can track either the exact particle orbit or the particle's gyro-centre. In this study, for performance reasons, TRANSP records the gyro-centres of fast deuterons. When Larmor orbits are sufficiently small, approximating the particle motion by its gyro-centre is generally acceptable. However, as the Larmor radius increases, finite Larmor radius effects may become significant. [35]

In such cases, the TOFOR neutron spectra can be affected, since some fast deuterons may exhibit Larmor radii of several centimetres. Specifically, the finite plasma volume observed by the TOFOR line of sight may not fully encompass the orbit of the fast deuterons around their gyro-centres. Due to the system geometry, some fast deuterons are effectively within the TOFOR line of sight when moving towards the detector, but move outside the field of view when moving away from it. If a fast deuteron undergoes a  $D(D,n)^3\text{He}$  reaction while moving towards the detector, the resulting neutron can be detected and will appear with an increased energy (due to energy and momentum conservation). Conversely, if the reaction occurs while the particle is moving away, the resulting neutron would be shifted to a lower energy, but is likely not observed because the particle has moved outside the line of sight. This asymmetry reduces the neutron yield in the low-energy region of the spectrum. Therefore, an orbit correction must be included in the calculations, where the full particle orbit is taken into account rather than just the gyro-centre.

The correction itself is relatively straightforward and was first introduced in [35]. Only the toroidal magnetic field  $B$  is considered and its value at each fast-deuteron gyrocentre is computed using

$$B = B_0 \frac{R_0}{R} \quad (2)$$

where  $B_0$  is the magnetic field on the magnetic axis,  $R_0$  the radial position of the magnetic axis, and  $R$  the radial position of the gyrocentre. The corresponding Larmor radius  $r_L$  was then obtained from

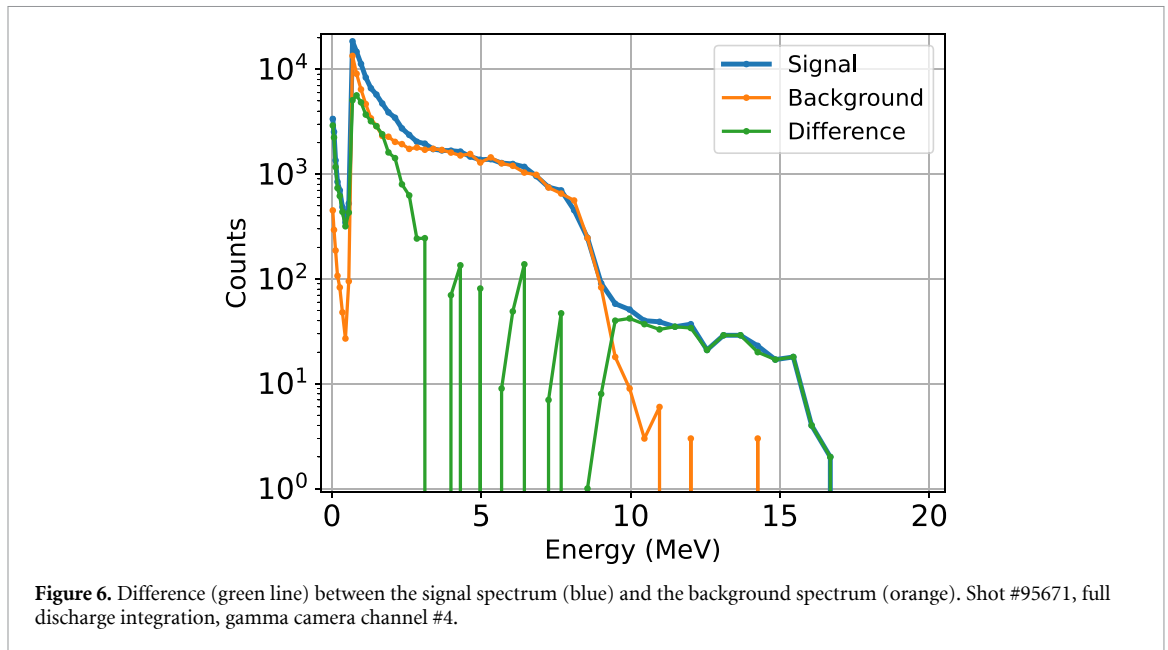
$$r_L = \frac{m_D v_\perp}{eB} \quad (3)$$

where  $v_\perp$  is the perpendicular velocity of the gyrocentre,  $e$  the proton charge, and  $m_D$  the deuteron mass. Knowing the Larmor radius, the particle position in the  $R$ - $Z$  plane can be computed by uniformly sampling the gyroangle.

Figure 5 shows the synthetic neutron energy spectra obtained from the orbit-corrected simulation of shot #95671 (ID A25) at 10 s. The Hfast-related components (blue, orange, and green lines) clearly dominate the spectral shape in both the high-energy ( $E_n > 3$  MeV) and low-energy ( $E_n < 2$  MeV) regions. This trend is consistent across the full discharge set, as expected from the enhanced fusion cross sections at energies above 100 keV.

#### 4.2. Alpha particle source

To reconstruct the alpha birth profile, it is necessary to model the alpha particle source in three-ions scheme experiments. The goal is to derive the alpha birth profile both from experimental observations



and from TRANSP-based simulations, enabling a direct comparison to evaluate the spatial predictive accuracy of the simulation.

In D-<sup>3</sup>He plasmas, alpha particles are produced via the <sup>3</sup>He(D,p)α fusion reaction. A less frequent branch of this reaction leads to the emission of a 16.4 MeV gamma ray through the <sup>3</sup>He(D,γ)<sup>5</sup>Li channel [30]. This gamma-ray emission, whose spatial profile provides a good approximation of that of fusion-born alpha particles from <sup>3</sup>He(D,p)α, can escape the plasma and be detected by the gamma camera at JET during three-ion scheme experiments, providing a means to assess the alpha birth profile.

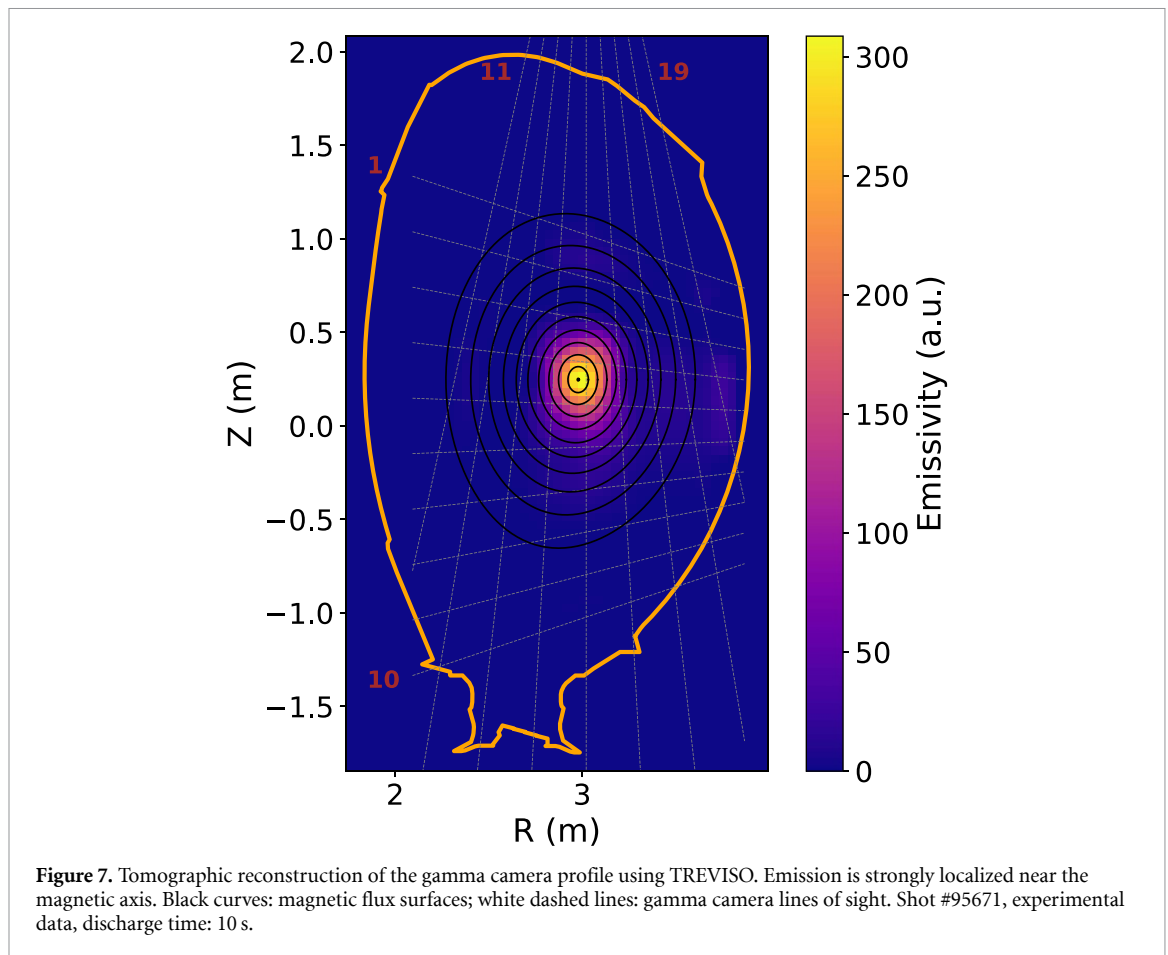
Our analysis begins with the extraction of experimental gamma camera profiles. These are then processed using the TREVISO code [24] to obtain a tomographic reconstruction of the alpha birth profile. The methods for deriving both experimental and synthetic gamma camera profiles are described in section 4.2.1, while the tomographic approach is presented in section 4.3.

#### 4.2.1. Processing experimental gamma camera data

Gamma camera data consist of a set of waveforms and the corresponding time stamps. When a gamma-ray is detected, its pulse shape is digitised in a waveform and the time of detection is stored in a time stamp. By analysing individual waveforms, using one of the algorithms described in [36], we can reconstruct the energy spectrum deposited in the crystal in any arbitrary time interval. In the discharges considered in this work the capability to resolve super-imposed pulses (pile-up) was particularly relevant to correctly reconstruct the shape of the spectrum in the high energy region of interest for alpha particle studies. A pile-up recovery algorithm has been recently implemented in a software named GetAGRaSp (Get A Gamma-Ray Spectrum) and used also to process the data analysed here. [18]

For all discharges listed in table 1, gamma camera binary files were retrieved and processed with GetAGRaSp to obtain reliable energy spectra for each gamma camera channel. Figure 6 shows an example of the gamma-ray spectrum measured by channel #4 in discharge #95671 and time integrated over the whole duration of the discharge. The spectrum comprises both high (say,  $E_\gamma > 10$  MeV) and low energy events, where the latter arise from the gamma-ray background induced by neutron interactions with the materials that surround the detectors. In order to eliminate such neutron induced background for our analysis, we have proceeded as it follows.

Each discharge follows a consistent heating sequence: NBI is activated at 6 s, followed by ICRH between 7.5 s and 12.5 s (see figure 2). The interval from 6 to 7.5 s, during which only NBI is active, is used to estimate the background. No significant 16.4 MeV gamma-ray emission is expected in this phase due to the lower deuteron energies involved, as also confirmed by our data. For each channel, a background spectrum is obtained by integrating over the NBI-only time window and averaging across the discharge set. The resulting spectrum is then normalised to the neutron yield of the pulse under analysis (obtained by the JET fission chambers), as shown by the orange line in figure 6, and subtracted from the corresponding signal spectrum during the ICRH phase, integrated over the desired time window.



The high-energy residual structure (green line in figure 6) reflects the interaction of 16.4 MeV gamma rays within the  $1'' \times 2/3''$  LaBr<sub>3</sub>:Ce detector [5, 10]. By integrating the background-subtracted spectrum above a 9 MeV threshold, the total gamma count per channel is obtained, providing the experimental gamma camera profile (an example is shown in figure 10).

#### 4.2.2. Synthetic gamma camera profiles

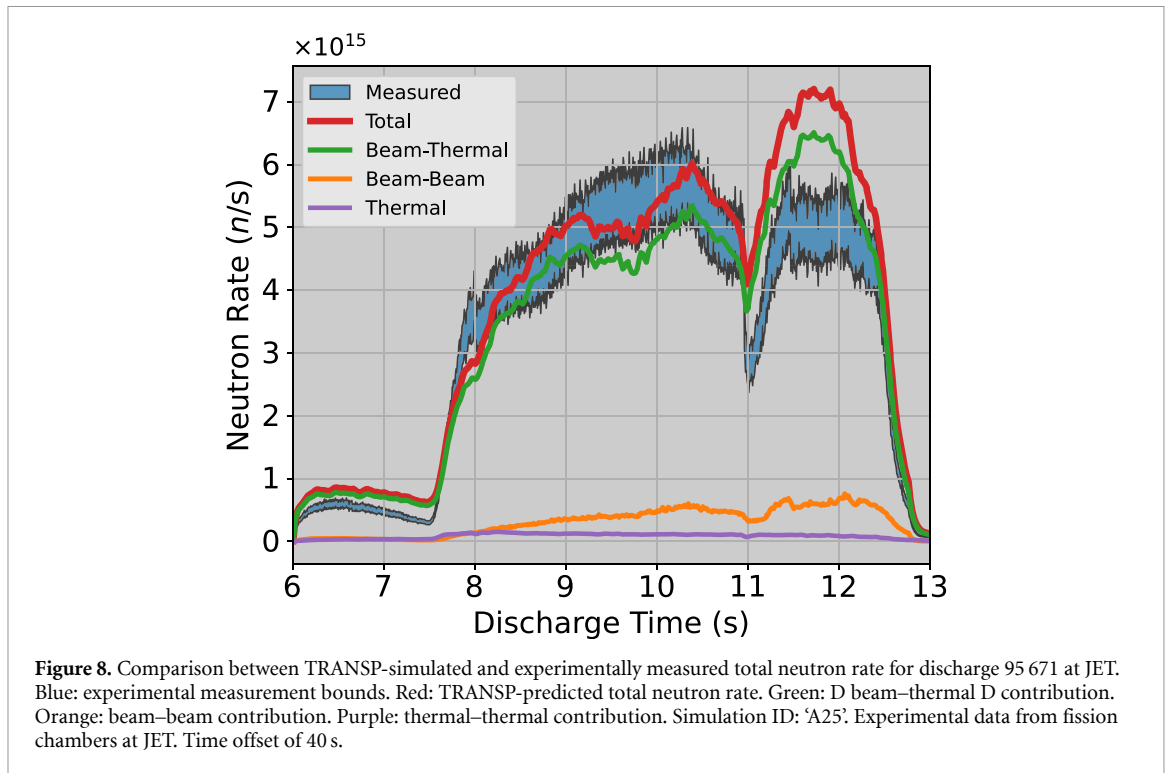
As indicated earlier, one way to validate TRANSP simulations of the deuterium distribution function and its spatial profile is to use this input to calculate synthetic gamma camera signal and to compare them with actual measurements.

To compute a synthetic gamma camera profile for comparison with experimental data, the fast deuterium distribution from TRANSP is used as input to the GENESIS code. This enables the numerical calculation of the gamma-ray emission expected from the  ${}^3\text{He}(\text{D},\gamma){}^5\text{Li}$  reaction in each gamma camera channel. As with the synthetic TOFOR spectra, the calculation of the gamma yield for each line of sight is performed in GENESIS, using the TRANSP fast deuterium distribution as input, along with the magnetic equilibria and helium-3 kinetic profiles. The 19 gamma camera line-of-sight files were calculated via the LINE 2.1 code [34].

### 4.3. Tomographic method

Starting from the actual gamma camera data, or corresponding synthetic signals evaluated from TRANSP results, we can determine the two-dimensional map of the gamma-ray emission in the poloidal plane by tomographic inversion.

To reconstruct a 2D poloidal map of the gamma-ray emissivity, and thus the alpha birth profile, we use the TREVISO code [24]. Specifically developed for gamma camera data at JET, TREVISO implements an iterative algorithm based on the maximum likelihood–expectation maximisation method to invert the line-integrated gamma camera signals into a pixel-based emissivity distribution. Magnetic equilibrium information is used to smooth the reconstructed emissivity along flux surfaces, enhancing the physical consistency of the results. This procedure is applied to both experimental and synthetic gamma camera profiles. An example is shown in figure 7.



For comparison purposes, the 2D emissivity maps are projected onto the normalized poloidal flux coordinate  $\rho$ . A  $\rho$  value is assigned to each pixel, and the emissivity values are then binned to produce a 1D emissivity profile. Two different procedures are used to derive the 1D profiles:

- **Synthetic data:** The simulated gamma camera profile is directly reconstructed using TREVISIO. After projection onto the  $\rho$  coordinate, pixel emissivity values are binned along the  $\rho$  axis. For each bin, the mean and standard deviation are computed, representing respectively the central value and uncertainty of the 1D profile.
- **Experimental data:** A similar procedure is applied, but over a set of one hundred gamma camera profiles derived from the original measurement. These profiles are generated using Poisson statistics, which govern counting processes. For each gamma camera channel, the original count  $N$  is used as the mean ( $\mu = N$ ) and the variance ( $\sigma^2 = N$ ) of the distribution. 100 synthetic profiles are then created by sampling from a Poisson distribution characterised by the previous parameters. This brute-force method allows propagation of statistical uncertainties through the tomographic reconstruction. The resulting error is combined quadratically with the reconstruction uncertainty to yield the final uncertainty of the 1D alpha birth profile.

## 5. Results

### 5.1. Total neutron rate time evolution

A comparison between the TRANSP-simulated and experimentally measured total neutron rate is used as an initial validation step for each simulation. A representative example is shown in figure 8.

As shown in figure 8, simulation 95 671A25 exhibits reasonable agreement with the experimental data up to the major sawtooth crash occurring at approximately  $t \approx 11$  s. A similar trend is observed across all discharges in the dataset, with a large sawtooth event occurring toward the end of each shot.

We do not expect the simulated and measured data after the sawtooth crash to agree since sawteeth eject fast ions with a velocity-space selective pattern [37]. We did not use a sawtooth crash model depleting the fast-ion population in the plasma centre in the TRANSP simulation. For this reason, the comparison between predictions and nuclear diagnostics data is limited to time intervals before the crash in all the discharges.

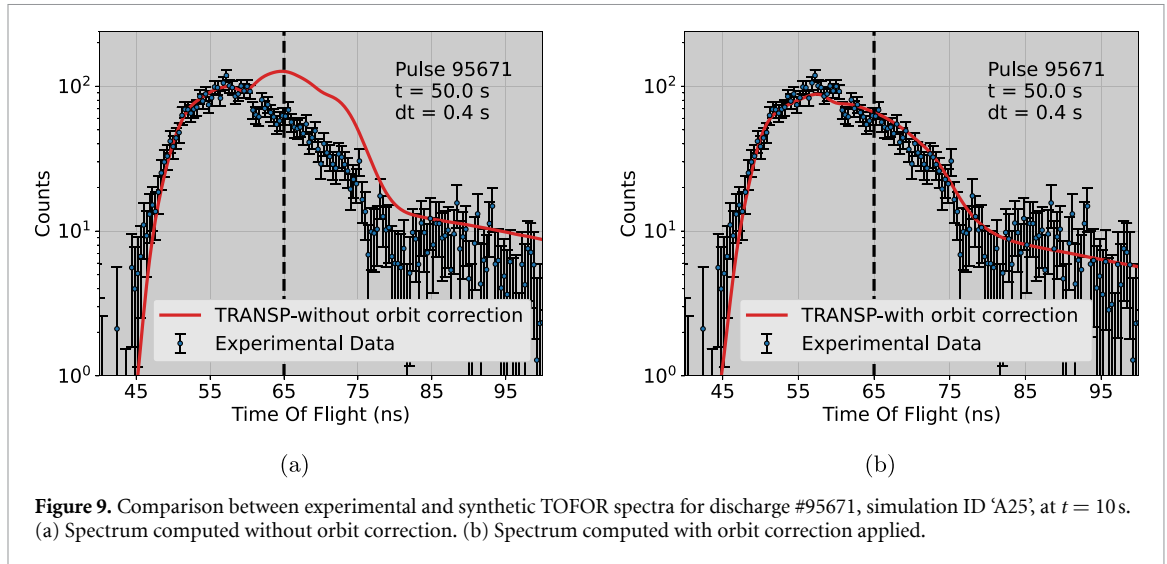


**Figure 9.** Comparison between experimental and synthetic TOFOR spectra for discharge #95671, simulation ID 'A25', at  $t = 10$  s. (a) Spectrum computed without orbit correction. (b) Spectrum computed with orbit correction applied.

The overall good agreement between the measured and modelled neutron rate before the sawtooth crash indicates that, when properly set up, TRANSP is capable of quantitatively reproducing the neutron rate time evolution with reasonable accuracy. For each discharge, we select the fast deuterium distribution calculated at the time points showing the best agreement with the measured neutron rate, as summarized in table 1.

### 5.2. Fast deuterium distribution and TOFOR spectra

Experimental neutron spectra from the TOFOR diagnostic were retrieved, and synthetic spectra were generated using the GENESIS code based on the TRANSP-calculated fast deuterium distribution, both with and without the application of the orbit correction procedure.

As shown in figure 9(a), the uncorrected synthetic spectrum exhibits good agreement with experimental data at low TOF values, corresponding to high neutron energies. However, a notable overestimation is observed at higher TOF values (lower energies).

Figure 9(b) displays the corresponding spectrum after applying orbit correction. In this case, a significantly improved match with the experimental data is obtained across the full TOF range. Similar results were observed for all analysed discharges, supporting the validity of the fast deuterium distribution from the selected TRANSP simulations in terms of spatial localization, energy distribution, and pitch-angle dependence.

### 5.3. Alpha birth profiles

Experimental gamma camera profiles were extracted and compared with synthetic profiles generated using GENESIS, with the TRANSP-derived fast deuterium distribution as input. Both profiles refer to the same time window. For direct comparison—and also because the gamma camera detectors are not absolutely calibrated—the synthetic profile was normalised to match the total gamma-ray counts of the experimental one.

As shown in figure 10, a good general agreement is observed between the experimental and synthetic profiles, consistently across all analysed discharges. The central channels (3–6 and 14–16), which intersect the plasma core, exhibit the strongest gamma-ray signals, indicating that the emission is concentrated near the plasma centre. Discrepancies in peripheral channels may result from localised vessel emissions or from background components not fully removed during processing.

Subsequently, the synthetic gamma camera profiles were reconstructed tomographically using the TREVISIO code. With the aid of magnetic equilibrium data, the resulting 2D emissivity maps were projected onto the normalised poloidal flux coordinate,  $\rho$ , to obtain 1D radial profiles, following the method described in section 4.3.

As illustrated in figure 11, the reconstructed emissivity profiles exhibit good consistency between experiment and simulation. In all cases, the alpha emission is strongly peaked at the plasma centre ( $\rho < 0.2$ ) and rapidly decreases, with the exact profile shape depending on the specific discharge. These results suggest that the simulation accurately represents the spatial distribution of alpha birth within the plasma core.

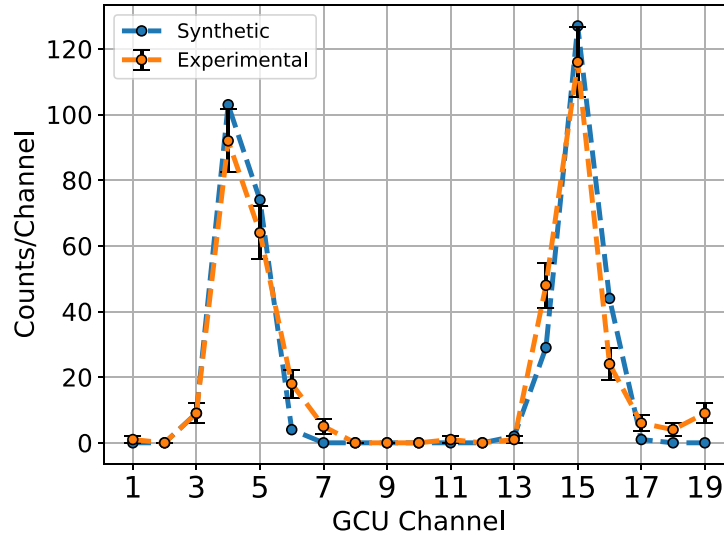


**Figure 10.** Comparison between experimental (orange) and synthetic (blue) gamma camera profiles. The synthetic profile is normalized to the total experimental gamma camera counts, for direct comparison. Error bars correspond to Poisson statistics (see section 4.3):  $\sigma = \sqrt{N}$ . Shot #95671, Simulation ID 'A25', discharge time: 10 s, Integration time:  $\pm 0.5$  s.

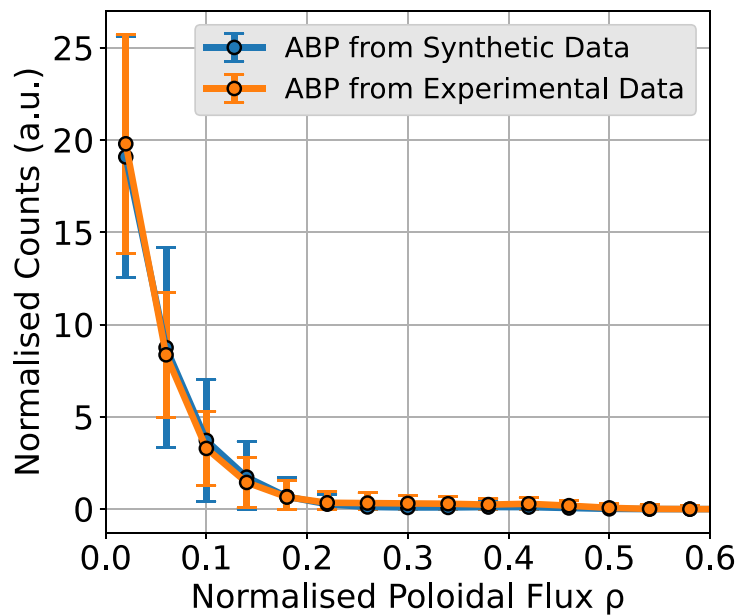
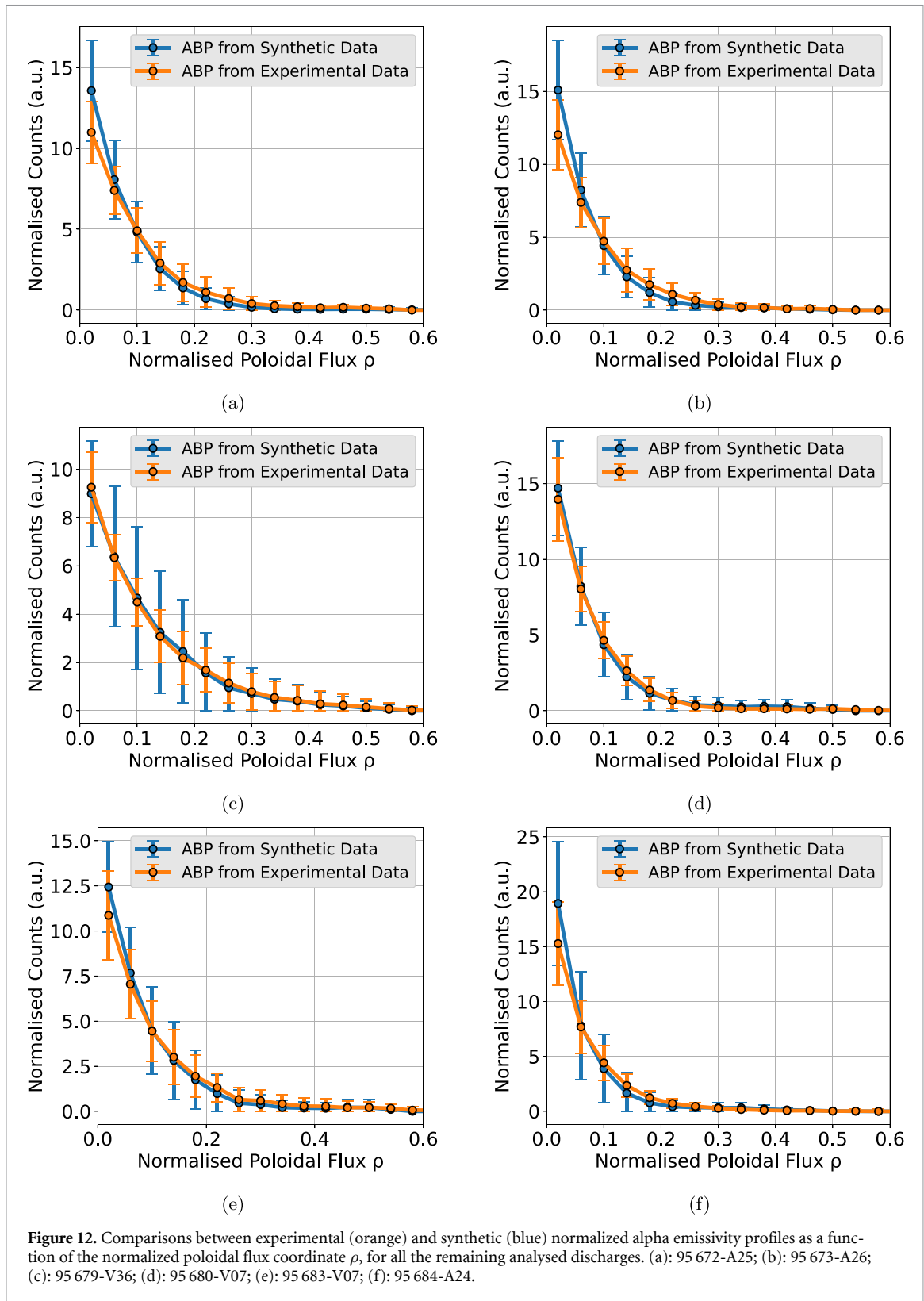


**Figure 11.** Comparison between experimental (orange) and synthetic (blue) normalized alpha emissivity profiles as a function of the normalized poloidal flux coordinate,  $\rho$ . See section 4.3 for error bar information. Shot #95671, Simulation ID 'A25', discharge time: 10 s.

It can be observed that the alpha birth profile derived from synthetic data in figure 11 generally exhibits larger error bars compared to the one obtained from experimental data. This is due to the greater spread in  $\rho$ -space of the pixels involved in the reconstruction of the synthetic gamma camera profile, compared to those contributing to the experimental profile.

## 6. Discussion

The results presented in this work indicate that, if properly configured (see section 4.1), TRANSP simulations at JET can effectively predict gamma and neutron emission from D-<sup>3</sup>He plasmas in three-ion scheme experiments. In particular, TRANSP provides time, space, energy and pitch-resolved distributions of the fast deuterium density, originating from NBI injection and further heated via ICRH. This fast component is primarily responsible for the localized and intense sources of gamma rays, neutrons, and alpha particles through fusion reactions. Based on the TRANSP fast D distribution, both emission



spectra and synthetic diagnostic profiles can be computed, enabling predictions for this class of experiments and deepening our understanding of three-ion scheme scenarios.

The neutron rate predicted by TRANSP is in acceptable agreement with experimental measurements, especially during the early phase of the discharge, prior to the major sawtooth crash occurring at  $\sim 11$  s in all analysed discharges. For this reason, timestamps for extracting the fast D distribution were selected in this early phase, where both the qualitative and quantitative behaviour of the neutron rate is in better agreement with fission chamber data at JET. The simulations confirm that neutron production

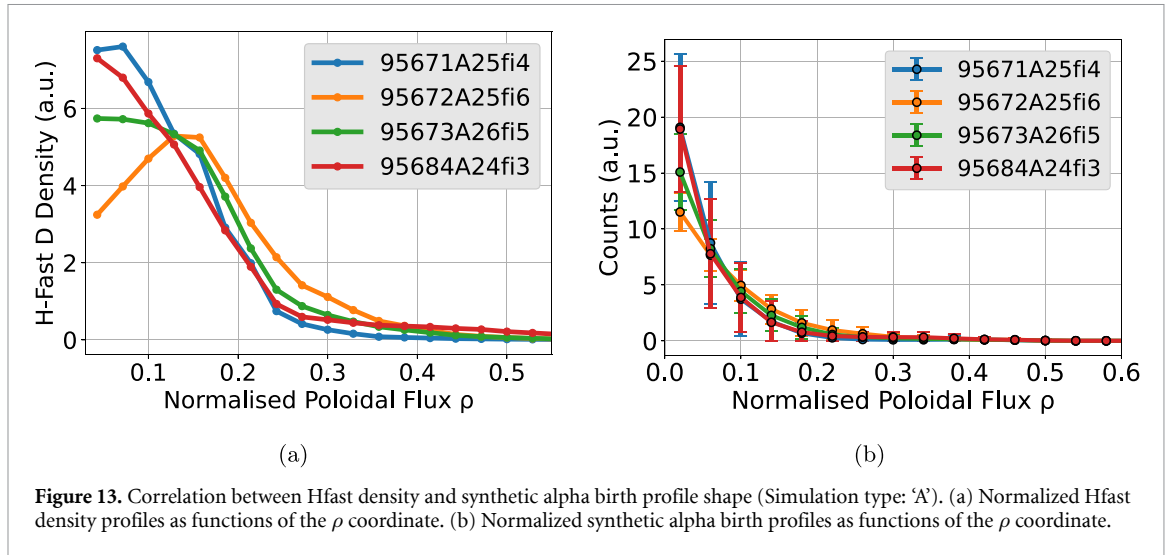


**Figure 13.** Correlation between Hfast density and synthetic alpha birth profile shape (Simulation type: ‘A’). (a) Normalized Hfast density profiles as functions of the  $\rho$  coordinate. (b) Normalized synthetic alpha birth profiles as functions of the  $\rho$  coordinate.

is primarily driven by the interaction between thermal deuterium and the fast deuterium population. This highlights the importance of accurately modelling the fast D distribution, as it plays a central role in interpreting three-ion scheme experiments. To produce a properly configured TRANSP simulation,  $^3\text{He}$  concentration variations, explored by incremental changes of about 5%, were used to identify the parameters required. In this three-ion heating scheme, due to the underlying physics mechanisms that determine the polarisation of the electric field, the neutron rate is very sensitive to the  $^3\text{He}$  concentration and variations of 5%–10% of the  $^3\text{He}$  concentration typically result in significant changes of the simulated neutron rate with respect to that measured.

TOFOR measurements offered an opportunity to test the TRANSP fast D distribution. Spectral features observed in the TOFOR data reflect corresponding structures in the simulated fast D distribution. By including finite Larmor radius effects in the synthetic spectra, a good agreement was obtained between TRANSP-based simulations and TOFOR data. In most discharges, the broad peak centred around 65 ns, typically attributed to thermal and NBI components, is not observed, suggesting a dominant contribution from the Hfast population (i.e. NBI deuterons effectively heated by ICRH). This component exhibits a broad and non-trivial spectral structure. Conversely, for discharge #95683, the peak associated with unheated NBI deuterons (with energies  $\lesssim 100\text{keV}$ ) interacting with thermal deuterium is clearly visible. This may indicate reduced ICRH heating effectiveness or comparatively lower ICRH power relative to NBI. Overall, TRANSP simulations facilitate the interpretation of the distinct components contributing to the neutron emission.

Gamma camera measurements offer a complementary spatial diagnostic for validating the fast D distribution. Using the TRANSP-derived fast D distribution as input, the poloidal distribution of alpha birth profiles can be numerically reconstructed and compared with tomographically inverted alpha birth profiles obtained from experimental gamma camera data. Across all analysed discharges, synthetic alpha birth profiles from TRANSP show reasonable agreement with the experimental reconstructions (figures 11 and 12). All cases exhibit a pronounced central peaking of emissivity near the magnetic axis, with a sharp drop-off at larger  $\rho$  values. Synthetic alpha birth profiles show a larger error due to the greater dispersion of the pixel into the  $\rho$ -space. The primary variation between discharges lies in the degree of central peaking relative to the outer plasma. TRANSP-derived fast D distributions help elucidate the connection between heating schemes and the resulting alpha birth profile shape.

A cross-analysis of normalized Hfast density profiles and synthetic alpha birth profiles as functions of the normalized poloidal flux  $\rho$  reveals a qualitative correlation (see figure 13). The sharper the Hfast density is peaked near the magnetic axis, the more pronounced the central peaking of the emissivity profile. In contrast, the Lfast component appears to have no significant impact on the alpha birth profile structure.

These observations suggest that TRANSP can be used not only for post-analysis but also for predictive purposes. In particular, controlling the heating scheme, especially the efficiency and spatial localization of ICRH, may allow shaping of the final alpha emissivity profile. This capability offers a pathway toward improved understanding and control of three-ions scheme experiments at JET and in future devices operating with D– $^3\text{He}$  plasmas.

Further investigations can include the quantitative evaluation in absolute units of the alpha particle intensity. Although beyond the scope of this work, this could be assessed in a similar manner to fusion power measurements performed at JET using DT gamma-ray detection via the TGRS system [13, 38–40]. As shown in section 4.2.1, 16.4 MeV gamma-rays from  ${}^3\text{He}(\text{D},\gamma){}^5\text{Li}$  reaction are easily observed in D– ${}^3\text{He}$  plasmas and, in principle, the corresponding fusion power (and, hence, the absolute intensity of the alpha particle source) can be determined from this emission. This is the only method to measure fusion power in D– ${}^3\text{He}$  plasmas because the D– ${}^3\text{He}$  reaction is aneutronic.

## 7. Conclusion

In this work, a set of D– ${}^3\text{He}$  discharges during Three–Ion Scheme experiments at JET has been analysed. For each discharge a TRANSP simulation has been performed, and outputs like the time evolution of the total neutron rate and the fast deuterium distribution have been retrieved and analysed. The aim was to validate the TRANSP outputs by producing synthetic neutron spectra and alpha particle birth profiles, comparing them against experimental results obtained from diagnostics like TOFOR and the gamma camera Upgrade at JET.

The time evolution of the total neutron rate predicted by TRANSP showed reasonable agreement with experimental data from the JET fission chambers. Synthetic spectra generated with GENESIS, based on the TRANSP-derived fast deuterium distribution, also showed good agreement with TOFOR measurements, especially when finite Larmor radius effects were included. Finally, the synthetic alpha birth profile, computed from the TRANSP fast deuterium distribution and reconstructed tomographically using the TREVISO code, was compared with the experimental alpha emissivity profile, showing acceptable agreement.

Moreover, the broader utility of TRANSP simulations has been discussed, highlighting their potential as a tool for improving the understanding of three-ions scheme experiments. In particular, TRANSP may help to optimise the heating scenarios, ultimately contributing to the development of efficient alpha particle sources based on the three–ion scheme for studies of alpha particles in plasmas without tritium and for tests of the diagnostics.

## Acknowledgments

This work has been carried out within the framework of the EUROfusion Consortium, funded by the European Union via the Euratom Research and Training Programme (Grant Agreement No 101052200 - EUROfusion). Views and opinions expressed are however those of the author(s) only and do not necessarily reflect those of the European Union or the European Commission. Neither the European Union nor the European Commission can be held responsible for them.

This scientific paper has been published as part of the international project co-financed by the Polish Ministry of Science and Higher Education within the programme called ‘PMW’.

## Data availability statement

Data will be made available on request.

## Funding

Eni SpA, Italy, provides support for this work through the PhD scholarships of Simone Lorenzo Fugazza and Marco Dalla Rosa.







## Author contributions

Simone Lorenzo Fugazza  0009-0006-0066-2612

Data curation (equal), Formal analysis (equal), Investigation (equal), Methodology (equal), Software (equal), Validation (equal), Visualization (lead), Writing – original draft (lead)

Marco Dalla Rosa  0009-0001-3360-7488

Data curation (equal), Formal analysis (equal), Investigation (equal), Software (lead), Writing – review & editing (equal)

- Enrico Panontin  [0000-0002-1309-0055](#)  
Formal analysis (equal), Methodology (equal), Software (equal)
- Andrea Dal Molin  [0000-0003-0471-1718](#)  
Conceptualization (equal)
- Jacob Eriksson  [0000-0002-0892-3358](#)  
Data curation (equal), Resources (equal), Software (equal)
- Giuseppe Gorini  [0000-0002-4673-0901](#)  
Project administration (equal), Supervision (equal)
- Yevgen Kazakov  [0000-0001-6316-5441](#)  
Conceptualization (equal)
- Vasily Kiptily  [0000-0002-6191-7280](#)  
Conceptualization (equal)
- Michal Poradzinski  [0000-0002-1858-4046](#)  
Resources (equal), Software (equal), Writing – review & editing (equal)
- John Rice  [0000-0001-8319-5971](#)  
Conceptualization (equal)
- Davide Rigamonti  [0000-0003-0183-0965](#)  
Conceptualization (equal)
- Mirko Salewski  [0000-0002-3699-679X](#)  
Conceptualization (equal), Writing – review & editing (equal)
- Žiga Štancar  [0000-0002-9608-280X](#)  
Resources (equal), Software (equal)
- Marco Tardocchi  [0000-0001-8443-1809](#)  
Project administration (equal), Supervision (equal)
- Massimo Nocente  [0000-0003-0170-5275](#)  
Conceptualization (lead), Funding acquisition (equal), Methodology (equal), Project administration (equal), Resources (equal), Software (equal), Supervision (lead), Validation (equal), Writing – review & editing (lead)

## References

- [1] Salewski M *et al* 2025 Energetic particle physics: chapter 7 of the special issue: on the path to tokamak burning plasma operation *Nucl. Fusion* **65** 043002
- [2] Mantica P *et al* 2024 Detection of alpha heating in JET-ILW DT plasmas by a study of the electron temperature response to ICRH modulation *Nucl. Fusion* **64** 086001
- [3] Kiptily V G *et al* 2023 Evidence of electron heating by alpha particles in JET deuterium-tritium plasmas *Phys. Rev. Lett.* **131** 075101
- [4] Nocente M *et al* 2022 Fusion product measurements by nuclear diagnostics in the Joint European Torus deuterium–tritium 2 campaign (invited) *Rev. Sci. Instrum.* **93** 093520
- [5] Nocente M *et al* 2020 Generation and observation of fast deuterium ions and fusion-born alpha particles in JET D-<sup>3</sup>He plasmas with the 3-ion radio-frequency heating scenario *Nucl. Fusion* **60** 124006
- [6] Kazakov Y O *et al* 2021 Physics and applications of three-ion ICRF scenarios for fusion research *Phys. Plasmas* **28** 020501
- [7] Kazakov Y O *et al* 2020 Plasma heating and generation of energetic D ions with the 3-ion ICRF + NBI scenario in mixed H-D plasmas at JET-ILW *Nucl. Fusion* **60** 112013
- [8] Reman B C G *et al* 2025 Velocity-space tomography of an MeV fast-ion tail generated by three-ion scheme ICRF heating at JET *Nucl. Fusion* **65** 076007
- [9] Kirov K K *et al* 2020 Synergistic ICRH and NBI heating for fast ion generation and maximising fusion rate in mixed plasmas at JET *AIP Conf. Proc.* **2254** 030011
- [10] Panontin E *et al* 2021 First spatially resolved measurements of the D-<sup>3</sup>He  $\alpha$ -particle source with the upgraded JET gamma-ray camera *Rev. Sci. Instrum.* **92** 053529
- [11] Rigamonti D *et al* 2018 The upgraded JET gamma-ray cameras based on high resolution/high count rate compact spectrometers *Rev. Sci. Instrum.* **89** 10I116
- [12] Zoita V *et al* 2009 Design of the JET upgraded gamma-ray cameras *Fusion Eng. Des.* **84** 2052–7
- [13] Nocente M *et al* 2021 A new tangential gamma-ray spectrometer for fast ion measurements in deuterium and deuterium-tritium plasmas of the Joint European Torus *Rev. Sci. Instrum.* **92** 043537
- [14] Nocente M *et al* 2013 High resolution gamma ray spectroscopy at MHz counting rates with LaBr<sub>3</sub> scintillators for fusion plasma applications *IEEE Trans. Nucl. Sci.* **60** 1408–15
- [15] Nocente M *et al* 2010 Energy resolution of gamma-ray spectroscopy of JET plasmas with a LaBr<sub>3</sub> scintillator detector and digital data acquisition *Rev. Sci. Instrum.* **81** 10D321

- [16] Kiptily V G *et al* 2002  $\gamma$ -ray diagnostics of energetic ions in JET *Nucl. Fusion* **42** 999
- [17] Iliasova M *et al* 2022 Gamma-ray measurements in  $D^3He$  fusion plasma experiments on JET *Nucl. Instrum. Methods Phys. Res. A* **1031** 166586
- [18] Nocente M *et al* 2020 MeV range particle physics studies in tokamak plasmas using gamma-ray spectroscopy *Plasma Phys. Control. Fusion* **62** 014015
- [19] Johnson M G *et al* 2006 The TOFOR neutron spectrometer and its first use at JET *Rev. Sci. Instrum.* **77** 10E702
- [20] Johnson M G *et al* 2008 The 2.5-MeV neutron time-of-flight spectrometer TOFOR for experiments at JET *Nucl. Instrum. Methods Phys. Res. A* **591** 417–30
- [21] Pankin A Y, Breslau J, Gorelenkova M, Andre R, Grierson B, Sachdev J, Goliyad M and Perumpilly G 2025 TRANSP integrated modeling code for interpretive and predictive analysis of tokamak plasmas *Comput. Phys. Commun.* **312** 109611
- [22] Grierson B A *et al* 2018 Orchestrating TRANSP simulations for interpretive and predictive tokamak modeling with OMFIT *Fusion Sci. Technol.* **74** 101–15
- [23] Štancar Ž *et al* 2023 Overview of interpretive modelling of fusion performance in JET DTE2 discharges with TRANSP *Nucl. Fusion* **63** 126058
- [24] Panontin E 2022 Development of nuclear radiation based tomography methods for runaway electrons and fast ions in fusion plasmas (Milano-Bicocca) Milano (available at: <https://boa.unimib.it/handle/10281/383194>)
- [25] Hellesen C, Giacomelli L and Johnson M G 2007 Measurement and analysis of the neutron emission from ICRH and NB heated JET D plasmas using the TOFOR spectrometer (available at: [www.osti.gov/etdeweb/biblio/20956169](http://www.osti.gov/etdeweb/biblio/20956169))
- [26] Valentini A, Reman B C G, Nocente M, Eriksson J, Järleblad H, Moseev D, Rud M, Schmidt B S, Snicker A and Salewski M 2024 A model for analytical calculations of synthetic neutron energy spectra from beam-target reactions *Nucl. Fusion* **65** 026001
- [27] Valentini A, Reman B C G, Nocente M, Eriksson J, Järleblad H, Moseev D, Rud M, Snicker A and Salewski M 2024 Relativistic calculations of neutron and gamma-ray spectra from beam-target reactions in magnetized plasmas *Rev. Sci. Instrum.* **95** 083551
- [28] Jacobsen A S, Binda F, Cazzaniga C, Eriksson J, Hjalmarsson A, Nocente M, Salewski M and Tardini G 2017 Velocity-space sensitivities of neutron emission spectrometers at the tokamaks JET and ASDEX Upgrade in deuterium plasmas *Rev. Sci. Instrum.* **88** 073506
- [29] Nocente M *et al* 2016 Gamma-ray spectroscopy at MHz counting rates with a compact  $LaBr_3$  detector and silicon photomultipliers for fusion plasma applications *Rev. Sci. Instrum.* **87** 11E714
- [30] Tilley D R *et al* 2002 Energy levels of light nuclei  $A = 5, 6, 7$  *Nucl. Phys. A* **708** 3–163
- [31] Felton R *et al* 2005 Real-time measurement and control at JET experiment control *Fusion Eng. Des.* **74** 561–6
- [32] Yang D K *et al* 2022 Simulations of neutral beam injection and ion cyclotron resonance heating synergy in high power EAST scenarios *Rev. Sci. Instrum.* **93** 113501
- [33] Nocente M 2012 Neutron and gamma-ray emission spectroscopy as fast ion diagnostics in fusion plasmas Milano-Bicocca (available at: <https://boa.unimib.it/handle/10281/28397>)
- [34] Hägg L *et al* 2023 Estimating the neutron yield in a deuterium plasma with the JET neutron camera *Rev. Sci. Instrum.* **94** 073502
- [35] Eriksson J, Hellesen C, Andersson Sundén E, Ceconello M, Conroy S, Ericsson G, Gatu Johnson M, Pinches S D, Sharapov S E and Weiszflog M 2012 Finite Larmor radii effects in fast ion measurements with neutron emission spectrometry *Plasma Phys. Control. Fusion* **55** 015008
- [36] Rosa M D 2023 Development of nuclear techniques for gamma-ray spectroscopy in thermonuclear plasmas *Master's Thesis* (Milano-Bicocca)
- [37] Salewski M *et al* 2016 High-definition velocity-space tomography of fast-ion dynamics *Nucl. Fusion* **56** 106024
- [38] Rebai M *et al* 2024 First direct measurement of the spectrum emitted by the  $^3H(^2H,\gamma)^3He$  reaction and assessment of the relative yield  $\gamma_1$  to  $\gamma_0$  *Phys. Rev. C* **110** 014625
- [39] Molin A D *et al* 2024 Measurement of the gamma-ray-to-neutron branching ratio for the deuterium-tritium reaction in magnetic confinement fusion plasmas *Phys. Rev. Lett.* **133** 055102
- [40] Marcer G *et al* 2025 Absolute measurement of the deuterium-tritium reaction gamma-ray emission in magnetic confinement fusion plasmas *Nucl. Fusion* **65** 086036